Nonlinear Dynamic Modeling and Analysis of Self-Oscillating H-Bridge Parallel Resonant Converter Under Zero Current Switching Control: Unveiling Coexistence of Attractors

A. El Aroudi, *Senior Member, IEEE*, L. Benadero, E. Ponce, C. Olalla, *Member, IEEE*, F. Torres, L. Martinez-Salamero, *Senior Member, IEEE*

***Abstract*—This paper deals with the global dynamical analysis of an H-bridge Parallel Resonant Converter (PRC) under a Zero Current Switching (ZCS) control. Due to the discontinuity of the vector field in this system, sliding dynamics may take place. Here, the sliding set is found to be an escaping region. Different tools are combined for studying the stability of oscillations of the system. The desired crossing limit cycles are computed by solving their initial value problem and their stability analysis is performed using Floquet theory. The resulting monodromy matrix reveals that these cycles are created according to a smooth cyclic-fold bifurcation. Under parameter variation, an unstable symmetric crossing limit cycle undergoes a crossing-sliding bifurcation leading to the creation of a symmetric unstable sliding limit cycle. Finally, this limit cycle undergoes a double homoclinic connection giving rise to two different unstable asymmetric sliding limit cycles. The analysis is performed using a piecewise-smooth dynamical model of a Filippov type. Sliding limit cycles divide the state plane in three basins of attraction and hence different steady-state solutions may coexist which may lead the system to start-up problems. Numerical simulations corroborate the theoretical predictions, which have been experimentally validated.**

I. Introduction

RESONANT power converters are more advantageous than pulse width modulated (PWM) counterparts in terms of size, efficiency, low electromagnetic interference, reduced dc gain variation, improved phase margin at high frequencies and simplicity of their control. Their ability to operate efficiently with high switching frequencies allows the use of small storage components and therefore increases the power density. Besides their traditional use in inductive heating, resonant converters are becoming increasingly popular in many applications such as efficient lighting [1], battery chargers in electrical vehicle [2] and wireless power transfer [3] among others [4], [5]. However, their dynamic behavior analysis is more involved due to their increased harmonic content. The dependence of their dynamics, both local and global, with the load is another problem of these converters.

Indeed, the assumption that the switching frequency is much higher than all the natural frequencies of the system, widely used in classical PWM converters, is no longer valid in resonant converters because their operating switching frequency is close to the natural frequency of the resonant circuit [6]. Consequently more advanced modeling tools such as the frequency-domain-based describing function [7]–[9] or the equivalent time-domain-based Hamel locus [10] are needed to describe the dynamics of the system. Discrete-time modeling is another accurate tool which were used in [3] to determine the possible steady-state operating points of an LCL wireless power transfer resonant converter. A similar approach was also used in [11], [12] to study the stability of the desired limit cycles in a series resonant power converter and a parallel LC resonant converter respectively. All the previous approaches assume a beforehand known switching pattern ignoring any possibility for sliding-motion to take place. This makes them to fail short in revealing the real global dynamics of the system. Namely, under the existence of sliding conditions, sliding motion can take place in this kind of systems [13], [14]. In particular, a trajectory of the switched system can partly remain on a sliding-mode region associated with an infinite number of switching between two different subsystems and a part of a limit cycle may emerge on this region. Sliding bifurcations take place when a crossing limit cycle interact with the sliding-mode region [15]. Such dynamical behavior results in nonsmooth complex behaviors that cannot be described by the approaches detailed in [6], [7], [9]–[11].

The system studied in this paper is a dc-ac Parallel Resonant Converter (PRC) under ZCS control [8], [9]. This converter is particularly interesting since it is only a two-dimensional system that can be described by a piecewise linear model, yet exhibiting different types of limit cycles and coexistence of attractors. The fact that such a simple low dimensional

A. El Aroudi, C. Olalla and L. Martinez-Salamero are with Universitat Rovira i Virgili, Departament d'Enginyeria Electrònica, Elèctrica i Automàtica, Escola Tècnica Superior d'Enginyeria, 43007, Tarragona, Spain (e-mail:abdelali.elaroudi@urv.cat).

L. Benadero is with Universitat Politècnica de Catalunya (UPC), Departament de Física, Barcelona, Spain.

E. Ponce and F. Torres are with Universidad de Sevilla, Instituto de Matemáticas (IMUS), Universidad de Sevilla (US), Sevilla, Spain.

This work has been sponsored by the Spanish Agencia Estatal de Investigación (AEI) and the Fondo Europeo de Desarrollo Regional (FEDER) under grant DPI2017-84572-C2-1-R (AEI/FEDER, UE) and also by the Spanish *Ministerio de Economía y Competitividad*, in the frame of project MTM2015-65608-P and by the *Consejería de Economía y Conocimiento de la Junta de Andalucía* under grant P12-FQM-1658.

Color versions of one or more of the figures in this paper are available online at http://ieeexplore.ieee.org

system can have such behavior indicates the importance of the study of piecewise linear systems. This work is then motivated by an attempt to accurately study the global nonsmooth and nonlinear dynamical behavior of the converter in terms of loading conditions. The generation of the different types of limit cycles that the system may have will be explained in the light of piecewise smooth dynamical systems and Filippov convex method [16], [17]. In particular, it will be shown that at the switching boundary an escaping sliding set exists that plays a key role in some limit cycle bifurcations and that under certain initial conditions, the circuit could not reach the desired crossing limit cycle.

The purpose here is to provide a sound approach to deal with this problem and to get a deep insight into the dynamics of the PRC. Some studies by the authors were presented in [18]–[20] where the strong dependence of the dynamics on the quality factor was demonstrated. In the present paper we thoroughly expand the previous analysis and fully explain the originally reported phenomena. An experimental validation of the results will also be provided. Moreover, the bifurcation patterns, which includes a cyclic-fold bifurcation (fold bifurcation of two limit cycles), a crossing-sliding bifurcation and a double homoclinic connection are extensively analyzed, getting a valuable information for the correct operation and design of the converter. From the results obtained in this paper, answers to the following questions will be given:

1) What kind of instability are possible in a PRC under ZCS control?
2) Is there a closed-form condition for predicting such instability?
3) What is the minimum value of load resistance for the system to exhibit stable oscillations?
4) What is the minimum value of load resistance guaranteeing convergence to the desired limit cycle with zero initial conditions?

The rest of this paper is organized as follows. Section II presents the mathematical switched model of the system. In Section III, the equations describing the dynamics at the escaping sliding-mode region are derived. Simulations from the switched model are presented in Section IV for different values of the load resistance R, thus revealing different dynamical behaviors and inferring coexistence of steady-state solutions. Section V is devoted to a combined analytical-numerical approach to obtain the steady-state crossing limit cycles and their stability analysis using the Floquet theory combined with Filippov technique for crossing trajectories and obtaining the saltation matrices. The boundary of cyclic-fold bifurcation is located in the same section. The conditions for nonsmooth crossing-sliding limit cycle bifurcations are derived in Section VI. A summary of the bifurcation scenario in terms of the load resistance is presented in Section VII. Experimental measurements are presented in Section XIII. Finally, concluding remarks are drawn in the last section.

II. System description and modeling

Fig. 1 shows the circuit diagram of the system considered in this study which consists of an LC PRC under ZCS control

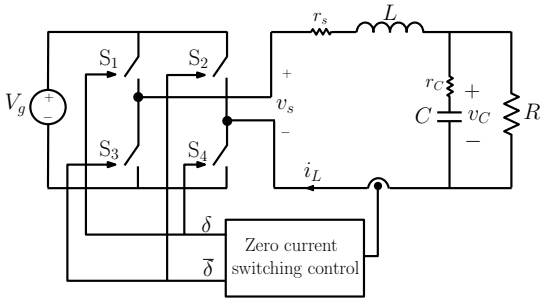

Fig. 1. Schematic circuit diagram of the LC PRC under ZCS control.

[8], [9]. Generally speaking, the PRC is a switched system that includes a resonant tank circuit and a switching network that actively participates in determining power flow. The switches S_1 and S_4 are ON (therefore $\delta = 1$, $\overline{\delta} = 0$ and $v_s = V_g$) when $i_L > 0$ and they are turned OFF (therefore $\delta = 0$, $\overline{\delta} = 1$ and $v_s = -V_g$) when $i_L < 0$. Note that the switches S_2 and S_3 are driven in a complementary way to S_1 and S_4.

Let v_C be the voltage of the output capacitor and i_L the inductor current. By applying KVL, the following dynamical model of the system is obtained

$$\frac{\mathrm{d}v_C}{\mathrm{d}t} = -\alpha\frac{v_C}{RC} + \alpha\frac{i_L}{C}, \tag{1a}$$

$$\frac{\mathrm{d}i_L}{\mathrm{d}t} = -\alpha\frac{v_C}{L} - \frac{\alpha r_C + r_s}{L} i_L + \frac{V_g}{L}u, \tag{1b}$$

where $\alpha = R/(R + r_C)$, C is the capacitance of the output capacitor with ESR r_C, L is the inductance of the inductor, R is the load resistance and V_g is the input source voltage. The resistance r_s encompasses the inductor and the switching devices energy dissipation.

All these parameters can be identified in the schematic circuit diagram of Fig. 1. The control strategy based on the use of the sign of the inductor current in the switching decision is called here ZCS control and should not be confused with the soft switching techniques used in power converters [21], [22]. In our case, the switching condition $h(v_C, i_L, t) = 0$ depends only of the inductor current i_L. The variable $u = 2\delta - 1$ is determined by the ZCS control strategy such that $u = 1$ (that is $\delta = 1$) if $i_L > 0$, and $u = -1$ (that is $\delta = 0$) if $i_L < 0$. Let $\mathbf{x} = (v_C,\, i_L)^\intercal$ be the vector of the state variables of the power stage, then the state-space model of the converter can be expressed as follows

$$\dot{\mathbf{x}} = \mathbf{A}\mathbf{x} + \mathbf{B}u, \tag{2a}$$

$$h(\mathbf{x}) = \mathbf{C}^\intercal\mathbf{x}, \tag{2b}$$

$$u = \mathrm{sign}(h(\mathbf{x})), \tag{2c}$$

where the matrix $\mathbf{A}$ and the vector $\mathbf{B}$ are given by

$$\mathbf{A} = \begin{pmatrix} -\dfrac{\alpha}{RC} & \dfrac{\alpha}{C} \\ -\dfrac{\alpha}{L} & -\dfrac{\alpha r_C + r_s}{L} \end{pmatrix}, \quad \mathbf{B} = \begin{pmatrix} 0 \\ \dfrac{V_g}{L} \end{pmatrix},$$

and $\mathbf{C}^\intercal = (0,\, 1)$, so that $h(\mathbf{x}) = i_L$. One has the following partitions in the state plane

$$\Sigma^+ = \{\mathbf{x} : h(\mathbf{x}) = \mathbf{C}^\intercal\mathbf{x} > 0\}, \quad u = 1, \tag{3a}$$

$$\Sigma^- = \{\mathbf{x} : h(\mathbf{x}) = \mathbf{C}^\intercal\mathbf{x} < 0\}, \quad u = -1. \tag{3b}$$

Note that at the switching boundary Σ, the driving signal u jumps between its two possible values 1 and -1. Hence, in accordance with the ZCS control, the system (2a)-(2c) can be rewritten as $\dot{\mathbf{x}} = \mathbf{F}(\mathbf{x})$, where $\mathbf{F}(\mathbf{x})$ is given by

$$\mathbf{F}(\mathbf{x}) = \begin{cases} \mathbf{F}^+(\mathbf{x}) = \mathbf{A}\mathbf{x} + \mathbf{B} \text{ in } \Sigma^+, \\ \mathbf{F}^-(\mathbf{x}) = \mathbf{A}\mathbf{x} - \mathbf{B} \text{ in } \Sigma^-. \end{cases} \tag{4}$$

Remark 1: *The vector field* $\mathbf{F}$ *is odd-symmetric,* i.e., $\mathbf{F}(-\mathbf{x}) = -\mathbf{F}(\mathbf{x})$. *Therefore, if* $\mathbf{x}_1(t)$ *is a limit set, then, either* $\mathbf{x}_1(t)$ *is asymmetric and there exists another solution* $\mathbf{x}_2(t)$ *given by* $\mathbf{x}_2(t) = -\mathbf{x}_1(t)$ *or* $\mathbf{x}_1(t)$ *is a unique symmetric solution with half period odd symmetry,* i.e., $\mathbf{x}_1(t) = -\mathbf{x}_1\left(t \pm \frac{T}{2}\right)$.

Each vector field is linear and time-invariant and the corresponding system of state equations can be solved in closed-form. Provided that the matrix $\mathbf{A}$ is invertible, the trajectory $\mathbf{x}(t)$ of the system at time t, starting from an initial condition $\mathbf{x}(t_c)$ at time instant t_c, can be expressed as follows

$$\mathbf{x}(t) = \mathbf{\Phi}(t - t_c)\mathbf{x}(t_c) \pm \mathbf{\Psi}(t - t_c) \tag{5}$$

where $\mathbf{\Phi}(t) = e^{\mathbf{A}t}$, $\mathbf{\Psi}(t) = \mathbf{A}^{-1}(\mathbf{\Phi}(t) - \mathbf{I})\mathbf{B}$, and $\mathbf{I}$ is an identity matrix with appropriate dimensions.

The equilibria of both vector field $\mathbf{F}^{\pm}$ can be obtained from null field condition $\mathbf{F}^{\pm}(\mathbf{x}) = \mathbf{0}$ or, equivalently, since the matrix $\mathbf{A}$ is Hurwitz, by taking the limit $\lim_{t\to\infty} \mathbf{x}(t)$ in (5), noting that $\lim_{t\to\infty} \mathbf{\Phi}(t) = \mathbf{0}$ and therefore $\lim_{t\to\infty} \mathbf{\Psi}(t) = -\mathbf{A}^{-1}\mathbf{B}$. The equilibrium point corresponding to the vector field $\mathbf{F}^+(\mathbf{x})$ is given by

$$\mathbf{x}_q^+ = -\mathbf{A}^{-1}\mathbf{B} = \begin{pmatrix} V_q \\ I_q \end{pmatrix} = \begin{pmatrix} \dfrac{RV_g}{\alpha(R + r_C) + r_s} \\ \dfrac{V_g}{\alpha(R + r_C) + r_s} \end{pmatrix}, \tag{6}$$

while the one corresponding to $\mathbf{F}^-(\mathbf{x})$ is simply $\mathbf{x}_q^- = -\mathbf{x}_q^+$. Both equilibria are stable and located in the corresponding partition that is $\mathbf{x}_q^+ \in \Sigma^+$ and $\mathbf{x}_q^- \in \Sigma^-$, so they are natural real equilibria and can be attracting for some initial conditions.

III. The dynamics on the escaping sliding region

As it is well known, sliding-mode regime can take place in systems described by piecewise smooth vector fields. This dynamical behavior is produced in a subset of the switching manifold, at which the normal component of the two involved vector fields are of opposite directions. Thus, if both vector fields point inwards or outwards the switching surface, an attracting or an escaping sliding set takes place respectively. Considering (4), the sliding manifold can be expressed as

$$\Sigma^S = \left\{\mathbf{x} \in \Sigma : \mathbf{C}^\intercal\mathbf{F}^-(\mathbf{x})\mathbf{C}^\intercal\mathbf{F}^+(\mathbf{x}) \leq 0\right\}, \tag{7}$$

After simple algebra, one gets

$$\Sigma^S = \left\{\mathbf{x} : -\frac{V_g}{\alpha} \leq v_C \leq \frac{V_g}{\alpha}, i_L = 0\right\}. \tag{8}$$

Remark 2: *Let* $\mathbf{x}_b^+ = (V_g/\alpha, 0)^\intercal$ *and* $\mathbf{x}_b^- = (-V_g/\alpha, 0)^\intercal$ *the right and the left extreme points of the sliding set* Σ^S. *Hence, one has that* $\mathbf{C}^\intercal\mathbf{F}^+(\mathbf{x}_b^+) = 0$ *and* $\mathbf{C}^\intercal\mathbf{F}^-(\mathbf{x}_b^-) = 0$.

The sliding subset in the system is escaping because

$$\frac{\mathrm{d}i_L}{\mathrm{d}t} > 0 \text{ for } i_L > 0 \text{ and } \frac{\mathrm{d}i_L}{\mathrm{d}t} < 0 \text{ for } i_L < 0$$

This is in a clear contrast with sliding-mode controlled power converters for which the switching decision is dictated in such a way that when i_L is positive, its derivative is negative and viceversa, so that the fields $\mathbf{F}^+$ and $\mathbf{F}^-$ points inwards Σ^S. Escaping sliding motion has received less attention in the literature [23], [24], but plays a key role in organizing the state plane of the system under study as will be shown later.

According to the Filippov method [13], [14], the field in the sliding region can be expressed as a convex combination of the two piecewise fields, *i.e.,*

$$\mathbf{F}^S(\mathbf{x}) = \lambda\mathbf{F}^+(\mathbf{x}) + (1 - \lambda)\mathbf{F}^-(\mathbf{x}), \quad \mathbf{x} \in \Sigma^S. \tag{9}$$

Therefore, trajectories on the sliding set located between its extreme points are solution of the Filippov vector field $\mathbf{F}^S$, which can be obtained by substituting λ with an equivalent control $\lambda_{eq} \in [0, 1]$ which is the smooth control law that would make Σ^S a local invariant manifold of the switched system, that is the solution of the equation $\dot{h}(\mathbf{x}) := \mathbf{C}^\intercal\mathbf{F}^S(\mathbf{x}) = 0$ in (9). Therefore, if $\lambda_{eq}(\mathbf{x})$ exists, its expression is given by

$$\lambda_{eq}(\mathbf{x}) = \frac{\mathbf{C}^\intercal\mathbf{F}^-(\mathbf{x})}{\mathbf{C}^\intercal(\mathbf{F}^-(\mathbf{x}) - \mathbf{F}^+(\mathbf{x}))}, \tag{10}$$

requiring that $\mathbf{C}^\intercal(\mathbf{F}^- - \mathbf{F}^+) \neq 0$. For the PRC considered in this study, one has that

$$\mathbf{C}^\intercal(\mathbf{F}^-(\mathbf{x}) - \mathbf{F}^+(\mathbf{x})) = -\frac{2V_g}{L} \neq 0. \tag{11}$$

Hence, theoretically, sliding motion may exist and the equivalent control (10) becomes

$$\lambda_{eq} = \frac{1}{2}\left(1 + \frac{\alpha v_C}{V_g}\right). \tag{12}$$

By substituting λ_{eq} for λ in (9), the Filippov reduced-order model $\dot{\mathbf{x}} = \mathbf{F}^S(\mathbf{x})$ is obtained, where $\mathbf{F}^S(\mathbf{x})$ is given by the following expression

$$\mathbf{F}^S(\mathbf{x}) = \mathbf{A}\mathbf{x} + \left.\frac{\alpha v_C}{V_g}\mathbf{B}\right|_{\mathbf{x}\in\Sigma^S} = \begin{pmatrix} -\dfrac{\alpha v_C}{RC} \\ 0 \end{pmatrix}. \tag{13}$$

It can be observed that the origin is an attractive equilibrium point for the ideal sliding dynamics and it is a pseudo-saddle for the switched system, since the sliding-mode region is escaping *i.e.,* trajectories evolve on Σ^S according to (13), but also escape into the regions Σ^+ and Σ^-.

IV. The crossing switching dynamics. Simulations from the switched model

The construction of the state plane trajectories for the switched vector field greatly facilitates the study of the global dynamics and it will therefore be used in the sequel. The trajectories corresponding to different values of the load resistance R will reveal different dynamical behaviors. Therefore, the dynamics will be explored by varying this parameter while maintaining the rest of the parameters fixed. The values of these parameters are depicted in Table I which also correspond to an experimental prototype that was built to validate the theoretical results. The resulting oscillation frequency of the PRC is in the range (500–570) kHz depending on the

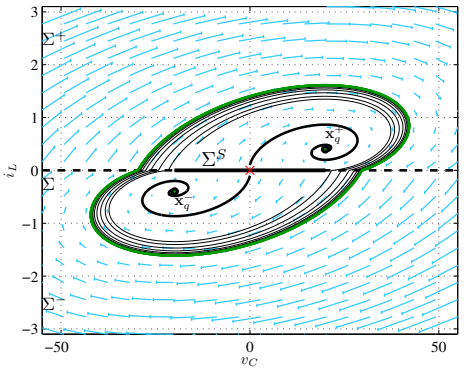

Fig. 2. Two pairs of symmetric orbits, which start near the unstable sliding-mode region Σ^S, evolving around the equilibria in the state plane (v_C, i_L). Observe that one pair tend to the corresponding equilibrium and the other pair cross the switching manifold Σ, so tending to a limit cycle. $R = 50\ \Omega$.

TABLE I
THE USED PARAMETER VALUES FOR THE SELF-OSCILLATING PRC.

V_g	L	r_L	C	r_C
20 V	7.3 μH	0.1 Ω	10.7 nF	1 mΩ

load resistance. The experimental results will be separately presented in Section IX.

In Fig. 2, two pairs of symmetric orbits evolving around the equilibria (dots) in the plane (v_C, i_L) are depicted. The starting points for all the orbits have been selected close to the unstable sliding set Σ^S. For one pair of symmetric orbits, the initial conditions have been chosen such that they do not reach the switching manifold Σ, hence tending to the corresponding equilibria. Conversely, for the other pair, the initial conditions have been selected in such a way that the trajectories cross the switching manifold Σ so that they will evolve to the corresponding limit cycle, which is made up of two symmetric pieces, one in each half state plane. Regarding the two kind of regular orbits plotted in Fig. 2, either flowing to an equilibrium or to a limit cycle, three different attractors may exist, hence, there must exist at least a boundary of attraction between the different limit sets. Trajectories starting outside the stable limit cycle will spiral towards the this limit cycle, hence, every point outside this limit cycle belongs to the basin of attraction of the same cycle. Trajectories in the interior of the stable limit cycle might converge to the same cycle, but they could spiral to any one of the stable equilibria either after hitting the switching boundary or without reaching it.

As will be shown later, the boundary between the basins of attraction of the different attractors might be an unstable crossing limit cycle, a sliding limit cycle interacting with the escaping sliding set Σ^S or two unstable sliding limit cycles.

V. DETERMINATION OF CROSSING LIMIT CYCLES AND THEIR STABILITY ANALYSIS

A. Computation of the crossing limit cycles

Let T be the period of the crossing limit cycle and let $\mathbf{x}_{ss}(0) = \mathbf{x}_{ss}(T)$ be the steady-state value of the state variables at the beginning/end of the switching cycle.

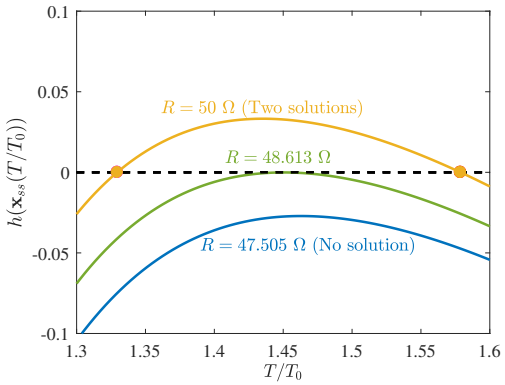

Fig. 3. The plot of the function $h(\mathbf{x}_{ss}(T))$ versus T/T_0 for three different values of R versus the steady-state normalized switching period.

Let $\mathbf{x}_{ss}(T/2)$ be the steady-state value of the state variables at time instant $T/2$. According to (5), $\mathbf{x}_{ss}(T)$ is given by

$$\mathbf{x}_{ss}(T) = \mathbf{\Phi}\left(\frac{T}{2}\right)\mathbf{x}_{ss}\left(\frac{T}{2}\right) - \mathbf{\Psi}\left(\frac{T}{2}\right), \quad (14)$$

and due to the odd symmetry of the vector field $\mathbf{F}$

$$\mathbf{x}_{ss}\left(\frac{T}{2}\right) = -\mathbf{x}_{ss}(T). \quad (15)$$

Putting (15) into (14), solving for $\mathbf{x}_{ss}(T)$ and imposing the switching condition $h(\mathbf{x}_{ss}(T)) := \mathbf{C}^\intercal \mathbf{x}_{ss}(T) = 0$ one obtains

$$\mathbf{x}_{ss}(T) = -\left(\mathbf{I} + \mathbf{\Phi}\left(\frac{T}{2}\right)\right)^{-1}\mathbf{\Psi}\left(\frac{T}{2}\right), \quad (16a)$$

$$h(\mathbf{x}_{ss}(T)) = \mathbf{C}^\intercal \mathbf{x}_{ss}(T) = 0. \quad (16b)$$

A solution of the equation $h(\mathbf{x}_{ss}(T)) = 0$ for T gives a steady-state switching period of a possible limit cycle. Note that the v_C-coordinate of $\mathbf{x}_{ss}(T)$ is negative. The plot of the function $h(\mathbf{x}_{ss}(T))$ is shown in Fig. 3 in terms of the steady-state normalized switching period T/T_0, $T_0 = 2\pi\sqrt{(R + r_C)LC/(R + r_s)}$ for different values of the load resistance R. This parameter defines the quality factor Q of the resonant tank according to the following expression

$$\frac{1}{Q} = \frac{Z_0 + \left(R(r_C + r_s) + r_C r_s\right)/Z_0}{\sqrt{(R + r_C)(R + r_s)}}, \quad (17)$$

and $Z_0 = \sqrt{L/C}$. It is clear that with $Q < 1/2$, the eigenvalues of the matrix $\mathbf{A}$ will be real, therefore, the response of each linear topology is overdamped and stable limit cycles cannot take place since the trajectories will at most cross the switching manifold once. In fact, stable limit cycles are born only for a quality factor $Q \approx 1.85$ corresponding to a load resistance $R = R_{\rm sn} \approx 48.613\ \Omega$ as can be appreciated in Fig. 3. For values of load resistance smaller than $R_{\rm sn}$, the equation $h(\mathbf{x}_{ss}(T)) = 0$ has no solution and therefore no limit cycle exists. On the contrary, for values of load resistance larger than $R_{\rm sn}$, the previous equation has two solutions and therefore two different crossing limit cycles can coexist in this case.

B. Stability analysis of crossing limit cycles

An approach for stability analysis of crossing limit cycles of switched systems is based on Floquet theory and the eigenvalues of the fundamental solution matrix over one complete cycle. This matrix is also called the monodromy matrix and its eigenvalues are called Floquet multipliers. For stability, all these eigenvalues must lie within the unit circle. The limit cycle is unstable if at least one eigenvalue is bigger than unity in absolute value. In piecewise linear systems, as is the case for the system considered in this study, the monodromy matrix can be constructed analytically and can be expressed as the product of the state transition matrices corresponding to each sub-cycle and the corresponding saltation matrices. It has been shown, using the Filippov method for crossing switching, that when the system switches from one vector field to another one and the switching condition $h(\mathbf{x}) = 0$ does not explicitly depend on time, the state transition matrix across the switching boundary, called also the saltation matrix $\mathbf{S}$ is given by [16], [17], [25]

$$\mathbf{S} = \mathbf{I} + \frac{(\mathbf{F}^{\text{after}}(\mathbf{x}(t_c)) - \mathbf{F}^{\text{before}}(\mathbf{x}(t_c)))\mathbf{C}^\intercal}{\mathbf{C}^\intercal \mathbf{F}^{\text{before}}(\mathbf{x}(t_c))}, \tag{18}$$

where $\mathbf{F}^{\text{before}}$ and $\mathbf{F}^{\text{after}}$ are, respectively, the vector fields before and after a switching taking place at time instant t_c. Within a switching cycle, two different switching take place. In steady-state these occur at the beginning/end of the period and its half. Then, one has two different saltation matrices which are given by

$$\mathbf{S}^+ = \mathbf{I} + \frac{(\mathbf{F}^+(\mathbf{x}_{ss}(T)) - \mathbf{F}^-(\mathbf{x}_{ss}(T)))\mathbf{C}^\intercal}{\mathbf{C}^\intercal \mathbf{F}^-(\mathbf{x}(T))}, \tag{19a}$$

$$\mathbf{S}^- = \mathbf{I} + \frac{(\mathbf{F}^-(\mathbf{x}_{ss}(\tfrac{T}{2})) - \mathbf{F}^+\left(\mathbf{x}_{ss}(\tfrac{T}{2})\right))\mathbf{C}^\intercal}{\mathbf{C}^\intercal \mathbf{F}^+(\mathbf{x}_{ss}(\tfrac{T}{2}))}. \tag{19b}$$

By using the expressions of the different vector fields, and taking into account that in steady-state one has that $\mathbf{x}_{ss}(T/2) = -\mathbf{x}_{ss}(T)$, the saltation matrices for the crossing limit cycles of the PRC become as follows

$$\mathbf{S}^- = \mathbf{S}^+ = \mathbf{S} = \mathbf{I} + \frac{2\mathbf{B}\mathbf{C}^\intercal}{\mathbf{C}^\intercal \mathbf{F}^-(\mathbf{x}_{ss}(T))} \tag{20}$$

Then, the monodromy matrix $\mathbf{M}$ corresponding to these limit cycles can be expressed as follows

$$\mathbf{M} = \mathbf{S}^+ \mathbf{\Phi}\left(\frac{T}{2}\right) \mathbf{S}^- \mathbf{\Phi}\left(\frac{T}{2}\right) = \left(\mathbf{S}\mathbf{\Phi}\left(\frac{T}{2}\right)\right)^2 \tag{21}$$

All the terms needed for calculating the monodromy matrix are therefore available in closed-form except the switching period T which must be computed numerically. For that, the value of T_0 can be used as an initial guess for solving the equation $\mathbf{C}^\intercal \mathbf{x}_{ss}(T) = 0$.

Remark 3: *Being the system two-dimensional, it has two Floquet multipliers of which one is expected to be always equal to one because the system is autonomous, which, as will be shown, implies that the remaining Floquet multiplier for each crossing limit cycle must be real and therefore Neimark-Sacker bifurcation cannot occur. Also, according to* (21)*, negative Floquet multipliers are not possible implying that period doubling cannot take place and that only cyclic-fold or symmetry breaking bifurcation can occur. The analysis of the limit cycles before and after the bifurcation point shows that it is a cyclic fold bifurcation.*

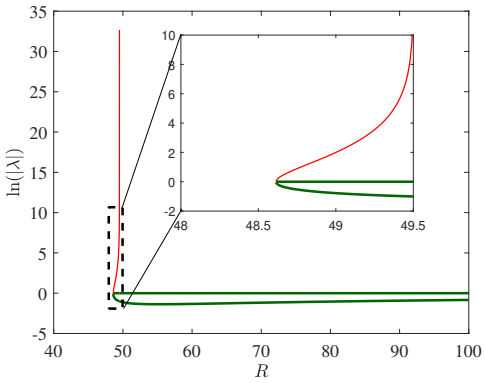

Fig. 4. Computed absolute values of the Floquet multipliers $|\lambda|$ of both the stable and the unstable limit cycles versus the load resistance of the PRC and a close view near the cyclic-fold bifurcation. For the stable limit cycle all the Floquet multipliers are within the unit circle one of them being always equal to one. For the unstable limit cycle, one of the Floquet multipliers becomes infinite when the sliding set is approached by this limit cycle.

Remark 4: *The saltation matrices become singular if* $\mathbf{C}^\intercal \mathbf{F}^+(\mathbf{x}) = 0$ *or symmetrically* $\mathbf{C}^\intercal \mathbf{F}^-(\mathbf{x}) = 0$*. For crossing limit cycles, generally, this will not happen. However, when the sliding set is approached by these limit cycles, this term becomes very small and consequently one of the Floquet multipliers will become very large.*

Fig. 4 shows the computed logarithm of the absolute values of the Floquet multipliers $\ln|\lambda|$ corresponding to the two computed crossing limit cycles when the load resistance is varied. This plot shows that one of the multipliers is always located at one independently of the value of the load resistance since the system is autonomous. As the value of this parameter approaches the critical value, the remaining eigenvalue for both limit cycles also approaches one indicating a cyclic-fold bifurcation. According to Remarks 1 and 4, one of the Floquet multipliers become infinite at $R \approx 49.505\ \Omega$ because close to this value, $\mathbf{x}_{ss}(T) \approx \mathbf{x}_b^+$ and equivalently $\mathbf{x}_{ss}(T/2) \approx \mathbf{x}_b^-$.

C. Derivation of cyclic-fold bifurcation boundary of the crossing limit cycles

Smooth cyclic-fold bifurcation is a local phenomenon which takes place when two limit cycles collide and annihilate each other. For the system considered in this study, at the boundary of this bifurcation, there is a tangency between the plot of $h(\mathbf{x}_{ss}(T))$ and the T-axis in such a way that two solutions of the equation $h(\mathbf{x}_{ss}(T)) = 0$ coalesce and disappear as shown before in Fig. 3. Therefore, the following two equalities hold simultaneously at this critical point

$$\mathbf{C}^\intercal \frac{\partial \mathbf{x}_{ss}(T)}{\partial T} = 0, \tag{22a}$$

$$\mathbf{C}^\intercal \mathbf{x}_{ss}(T) = 0. \tag{22b}$$

The partial derivative in (22a) can be obtained by using (16a) and differentiating the involved matrix functions, hence the equation (22a) becomes

$$\mathbf{C}^{\intercal}\left(\mathbf{I}+\mathbf{\Phi}\left(\frac{T}{2}\right)\right)^{-1}\mathbf{\Phi}\left(\frac{T}{2}\right)\mathbf{F}^{+}(\mathbf{x}_{ss}(T))=0. \qquad (23)$$

For the set of parameters values shown in Table I, the obtained solutions for T and R from the previous equations are $T \approx 2.54$ μs and $R = R_{\rm cs} \approx 48.613$ Ω in a perfect agreement with what was predicted from the switched model, with the static analysis whose results are depicted in Fig. 3 and also with the evolution of the Floquet multipliers in Fig. 4. It was observed that this critical value does not depend on the input voltage V_g. It mainly depends on the parameters defining the quality factor of the system such as the inductance of the inductor and the capacitance of the capacitor.

VI. Nonsmooth limit cycle bifurcations

A. Crossing-sliding boundary

The crossing limit cycles are characterized by the fact that $v_C(T) < -V_g/\alpha$. If, by varying a parameter, the conditions $v_C(T) = -V_g/\alpha$ and equivalently $v_C(T/2) = V_g/\alpha$ are fulfilled, the system limit cycle hits the sliding set Σ^S and sliding limit cycles take place. This phenomenon is called a crossing-sliding bifurcation which can be located by solving its initial value problem.

$$\mathbf{x}_{ss}(T)=\mathbf{x}_b^{-} \quad \text{or} \quad \mathbf{x}_{ss}\left(\frac{T}{2}\right)=\mathbf{x}_b^{+}. \qquad (24)$$

Once the period T is computed using (24), the v_C-coordinate for the corresponding limit cycle can be obtained by simply evaluating the trajectory at this time instant. With the set of parameter values depicted in Table I, the solution for the previous equation gives $R_{\rm cs} \approx 49.505$ Ω.

B. Sliding limit cycles

Let define the particular orbit in $\Sigma^+ \cup \Sigma$ for the linear field $\mathbf{F}^+$ that, starting at the switching manifold, reaches the extreme of the sliding set, $\mathbf{x}_b^+ = (V_g/\alpha, 0)^{\intercal}$ in a time t_{sb}. Due to the contractive character of $\mathbf{F}^+$, this orbit always exists, together with an equivalent symmetric orbit in $\Sigma^- \cup \Sigma$ that starts at Σ and addresses to $\mathbf{x}_b^- = (-V_g/\alpha, 0)^{\intercal}$. Let $\mathbf{x}_{sb} \in \Sigma$ and its symmetric $-\mathbf{x}_{sb}$ be the starting points of these orbits. If $\mathbf{x}_{sb}$ is located on the left of $\mathbf{x}_b^-$, that is outside Σ^S, then sliding cycles do not exist. If $\mathbf{x}_{sb}$ is located between $\mathbf{x}_b^-$ and the origin, then this orbit can be continued backwards in time on Σ^S to $\mathbf{x}_b^-$ and linked with its symmetric counterpart, thus defining a unique sliding limit cycle, encircling the origin and the two equilibrium. Actually, this unstable limit cycle is the boundary between the basins of attraction of the two equilibrium points. Finally, if $\mathbf{x}_{sb}$ is located between the origin and $\mathbf{x}_b^+$, then this orbit can be continued backwards in time on Σ^S to $\mathbf{x}_b^+$ itself, thus defining a sliding limit cycle which encircles the equilibrium point $\mathbf{x}_q^+$, thus defining the boundary of its basin of attraction. Also, in this case, a symmetric sliding limit cycle, which encircles $\mathbf{x}_q^-$ and is its boundary of attraction, exists.

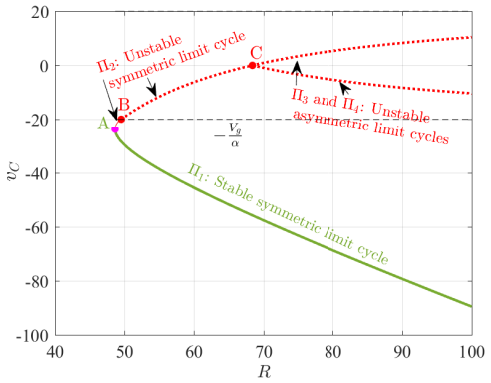

Fig. 5. Summary of the bifurcations as the load resistance is varied. For the crossing limit cycles, the evolution of the v_C-coordinate of the state vector $\mathbf{x}$ in terms of the load resistance R is shown. The birth of two different solutions can be appreciated at $R = R_{\rm sn} \approx 48.613$ Ω ($Q = Q_{\rm sn} \approx 1.850$). For the unstable sliding limit cycles, the evolution of the v_C-coordinate of the steady-state vector $\mathbf{x}_{ss}(t_{sb})$ is shown. A crossing-sliding bifurcation takes place at $R = R_{\rm cs} \approx 49.50$ Ω ($Q = Q_{\rm cs} \approx 1.883$) when $v_C(T) = -V_g/\alpha$ and equivalently $v_C(T/2) = V_g/\alpha$. At Point C, $R = R_{\rm hc} \approx 68.407$ Ω ($Q = Q_{\rm hc} Q \approx 2.595$), a double homoclinic connection takes place.

Taking int account the expression (5), the time t_{sb} and its corresponding point $\mathbf{x}_{sb}$ can be computed from the following condition

$$\mathbf{C}^{\intercal}\mathbf{x}_{sb}=\mathbf{C}^{\intercal}\mathbf{\Phi}^{-1}(t_{sb})(\mathbf{x}_b^{+}-\mathbf{\Psi}(t_{sb}))=0. \qquad (25)$$

Note that the critical case $\mathbf{x}_{sb} = \mathbf{x}_b^-$ corresponds to the crossing sliding bifurcation obtained from (24), in which $t_{sb} = T/2$. Therefore, unstable sliding limit cycles exist only for $R > R_{\rm cs}$.

C. Double homoclinic connection of sliding limit cycles

This phenomenon takes place when a single symmetric limit cycle bifurcates into two different asymmetric limit cycles [24], being the origin $\mathbf{0} = (0,0)^{\intercal}$ the only common point between them. Therefore, this boundary can be determined by solving the following equation

$$\mathbf{\Phi}^{-1}(t_{sb})(\mathbf{x}_b^{+}-\mathbf{\Psi}(t_{sb}))=\mathbf{0}. \qquad (26)$$

With the set of parameter values depicted in Table I, the solution for the previous set of equation gives $R_{\rm sb} \approx 68.407$ Ω. From a practical point of view, this is the minimum value of load resistance that will guarantee the convergence of the system to the desired crossing limit cycle starting from zero initial conditions.

VII. Summary of the bifurcation scenario in the PRC under ZCS control

To get clearer view of the behavior of the switched system, a bifurcation diagram is computed by using the descriptive equations of all the bifurcations described in the previous sections. The corresponding steady-state vector was computed and the switching condition was imposed. The bifurcation diagram when varying this parameter is depicted in Fig. 5 which shows four different branches with periodic solutions. In

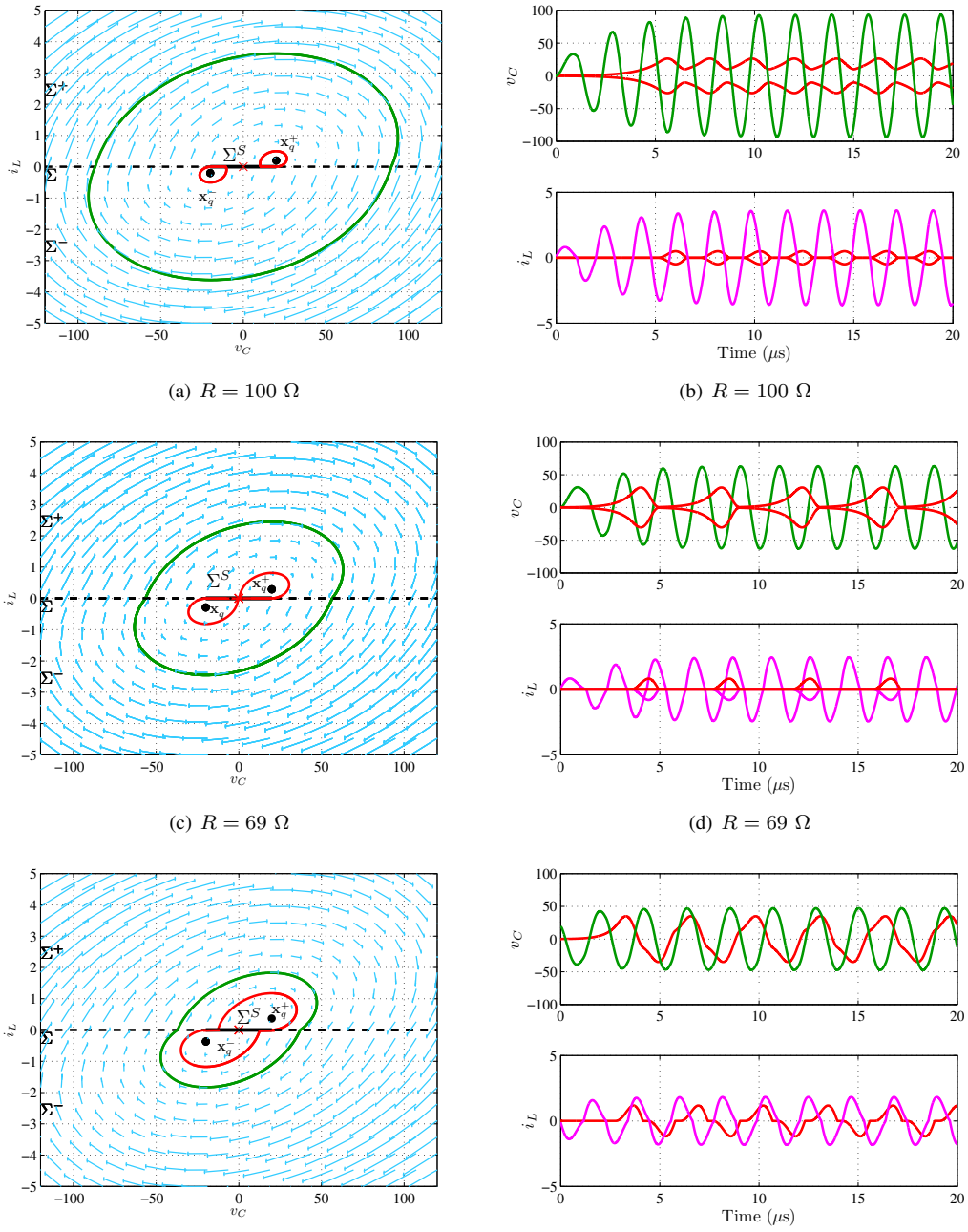

(a) $R = 100\ \Omega$ (b) $R = 100\ \Omega$

(c) $R = 69\ \Omega$ (d) $R = 69\ \Omega$

(e) $R = 54\ \Omega$ (f) $R = 54\ \Omega$

Fig. 6. Different crossing (stable) and sliding (unstable) limit cycles and their corresponding time-domain waveforms for different values of the load resistance. Because the sliding region and the sliding limit cycles themselves are unstable, it is not possible to compute them in forward time and calculation in backward time is needed. The escaping sliding region in the forward time becomes an attracting sliding region in backward time. For the cases (a)-(b) and (c)-(d) initial conditions close to the origin were used to reach the unstable sliding limit cycles in backward time and the stable crossing limit cycles in forward time. For the case (e)-(f) the stable crossing limit cycle cannot be reached from zero initial conditions and these have been therefore selected within the basin of attraction of the limit cycle.

that figure the v_C-coordinate is plotted against the bifurcation parameter R.

Branch Π_1 (thick) corresponds to the desired stable symmetric crossing limit cycle. For relatively small load resistance values, no periodic solution exits under ZCS control and are only created at the turning point A at which $R = R_{sn} \approx 48.613\ \Omega$. For sufficiently large load resistance values, the periodic solutions in Branch Π_1 are close to the ones corresponding to harmonic resonance in the linear LC tank with almost sinusoidal symmetric crossing limit cycles with output capacitor voltage amplitude approximately equal to $4QV_g/\pi$ being the switching frequency close to the resonant frequency in this case [8].

Branch Π_2 contains different types of limit cycles. Close to the turning point A, an unstable crossing limit cycle (thin) exists in a small range of the load resistance $R \in (R_{\rm sn}, R_{\rm cs})$, $R_{\rm cs} \approx 49.505\ \Omega$. If the load resistance increases, this limit cycle hits the sliding set at the critical point B where $R = R_{\rm cs}$ and sliding limit cycles take place (dotted). At this critical point, the crossing Branch Π_2 becomes infinitely unstable in the sense that one of the characteristic multipliers becomes infinite.

Unstable symmetric limit cycles on Branch Π_2 for values of the load resistance in the range $R_{\rm sn} < R < R_{\rm cs}$ between Point A and Point B do not contain sliding-mode regime. Unstable symmetric limit cycles on Branch Π_2 for $R_{\rm cs} < R < R_{\rm hc}$, $R_{\rm hc} \approx 68.407\Omega$, between Point B and Point C contain sliding-mode regime whose corresponding time during which the inductor current is zero interval increases with R. At $R \approx R_{\rm hc}$ the unstable limit cycle on Branch Π_2 is destroyed at the point C and two asymmetric sliding limit cycles are created forming the unstable branches Π_3 and Π_4.

To sum up, we have three different bifurcation points when the load resistance R is varied. These points correspond to three different values of R: $R_{\rm cf} \approx 48.613\ \Omega$ corresponding to a smooth cyclic-fold bifurcation, $R_{\rm cs} \approx 49.505\ \Omega$ to a border collision between a crossing and a sliding limit cycle and $R_{\rm hc} \approx 68.407\ \Omega$ which corresponds to a double homoclinic connection. Consequently, four regions having different limit sets can be clearly identified as shown in Fig. 5. Below, a description of the different cases is given and one example of state plane and time domain waveforms for some representative cases are represented in Fig. 6

1) For $R < R_{\rm cf}$, no limit cycles exist and the only steady-state stable solutions are the equilibrium points corresponding to the linear configurations of the switched system.
2) At $R = R_{\rm cf}$, the crossing limit cycles are created.
3) For $R_{\rm cf} < R < R_{\rm cs}$, two crossing limit cycles coexist. Orbits starting outside the inner unstable cycle converge to the outer stable limit cycle. The basin of attraction of each equilibrium point is defined by backward time orbits from the boundary of the sliding set.
4) At $R = R_{\rm cs}$, the unstable crossing limit cycle hits the sliding set and unstable sliding limit cycle is about to be created.
5) For $R_{\rm cs} < R < R_{\rm hc}$, apart from the outer stable crossing limit cycle, the unstable sliding limit cycle is unique and of sliding type, with a non-zero sliding time interval. The sliding-mode region inside the unstable limit cycle complete the boundary of the basin of attraction of the two equilibrium points. The origin does not belong to the basin of attraction of the desired crossing limit cycle. Initial conditions must be outside this basin for the system to reach the desired stable crossing limit cycle in steady-state. This case is represented in Fig. 6(e)-(f).
6) At $R = R_{\rm hc}$, the unstable crossing limit cycle is split onto two asymmetric sliding limit cycles (Fig. 6(c)-(d)).
7) For $R > R_{\rm hc}$, there are two unstable sliding limit cycles and one crossing stable limit cycle. The unstable cycles are the boundary of the basin of attraction of the corresponding equilibrium point. Trajectories starting outside these cycles converge to the desired stable limit cycle. Those starting inside these cycles spiral towards the corresponding equilibria. However, these cycles are so small that the probability for a trajectory to tend towards these equilibria is very small. Actually this case, which is represented in Fig. 6(a)-(b), is the one desired in regular applications, because the origin belongs to the basin of attraction of the stable limit cycle.

From a practical point of view, it is very helpful to know some of the previous critical parameter values. In particular, the determination of the onset of the smooth cyclic-fold bifurcation allows to know the feasible loading conditions for the system to exhibit desired stable oscillations while the determination of the double homoclinc connection corresponds to the minimum load resistance values guaranteeing the convergence to the desired crossing limit cycle from zero initial conditions.

It is worth mentioning here that the same phenomena are obtained regardless the values of the remaining fixed parameters such as the inductance L, the capacitance C and the input voltage V_g. Moreover, the variation of V_g does not alter the critical values of the load resistance where bifurcations take place.

VIII. Experimental results

A. Experimental setup

To validate the theoretical results and the numerical simulation, an experimental prototype of an H-bridge PRC, using the parameter values and components shown in Table I, has been implemented. The power stage consists of four MOSFETs (IPB200N15N3) activated by a circuit based on the driver UCC27210. The resonant capacitance corresponds to three parallel connected high-quality low-ESR NP0/CG0 capacitors. The resonant inductor has been realized in-house with a litz-wire winding on a coreless bobbin former, which results in very low losses. The efficiency of the resonant tank has been verified by measuring the experimental quality factor with a load resistance of 300 Ω. For this value, the difference in the quality factor between the theoretical value and the measured one was below 10%. The current sensor has been realized with a 1:20 current transformer. LT1394 comparators activate the desired branch of the full-bridge inverter depending on the control law. The schematic circuit diagram and a picture of the experimental prototype are shown in Fig. 7.

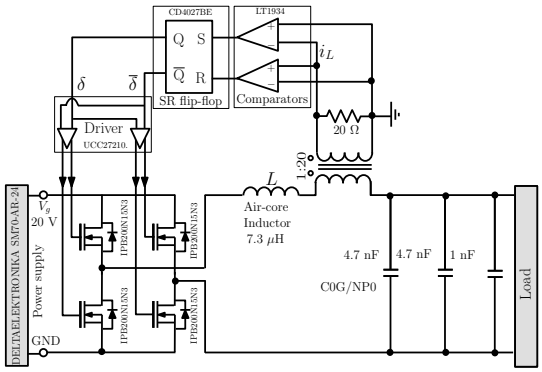

(a) Schematics circuit diagram.

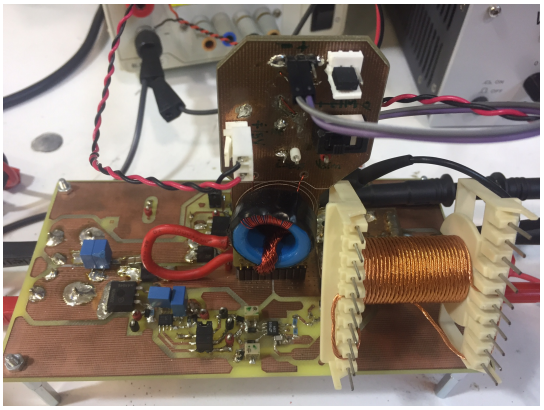

(b) Picture of the prototype.

Fig. 7. A picture and the schematic diagram of the experimental setup where the implemented PRC prototype.

B. Results

The load resistance was varied and the rest of parameters were fixed as in numerical simulations tests. Three values of load resistances were selected for validating the previous results. Namely, resistive loads with different resistance values were used. These are: $R = 54\ \Omega$, $R = 69\ \Omega$ and $R = 100\ \Omega$. The corresponding waveforms of the output capacitor voltage $v_o \approx v_C$ and the inductor current i_L are represented in Fig. 8 together with their corresponding state plane trajectories in steady-state. By observing the current waveforms in the oscilloscope, it could be observed that between the zero current crossing instant and the effective switching instant, there is a total delay of about 120 ns. Note that except from the effect of this propagation delay, there is a good agreement between the real measurements in Fig. 8 and the simulated system behavior depicted in Fig. 6. In particular, while it is possible to make the system to reach the desired crossing limit cycle for relatively high values of the load resistance, it is not the case when this parameter decreases.

IX. Conclusions

The asymptotic behavior of a self-oscillating H-bridge LC parallel resonant converter under a zero current switching control has been studied. Its dynamics has been explored by performing a bifurcation analysis with respect to the load resistance which, together with the values of the reactive components, determines the quality factor of the circuit. A general view of limit cycles in the system has been given by combining different analytical and numerical tools which have been used for studying different types of bifurcations of the system. Stability analysis of crossing limit cycles has been performed by using Floquet theory combined with Filippov method showing that these cycles may undergo a cyclic-fold bifurcation. Using a static approach and tangency condition, a closed-form condition is derived for the onset of this bifurcation. Then, the sliding-crossing bifurcation boundary has been located by solving its initial value problem. We have shown how one can proceed to obtain the entire bifurcation diagram proving that different kind of bifurcations, both smooth and nonsmooth, are possible in the system. In particular, a double homoclinic connection of sliding limit has been located. Different critical values of the load resistance have been determined. The mathematical analysis has shown that sufficiently high quality factors guarantee that the desired limit cycle can be reached even with zero initial conditions. However, for relatively low values of the quality factor, the effect of the coexistence of attractors is more prominent and starting at the basin of attraction of the desired limit cycle is necessary for the system to reach this cycle. The boundaries between the basins of attractors have been obtained by considering the escaping sliding-mode region in the switching manifold. Other converter topologies such as LCC, LLC, and LCLC among others either under zero current switching or zero voltage switching control strategies fit the modeling approach and the theory used and could be studied using an analysis similar to the one performed in this paper. Extending the results to these topologies as well as the effect of the propagation delay on the system behavior could be a topic of further study.

References

[1] P. D. Teodosescu, M. Bojan, and R. Marschalko, “Resonant LED driver with inherent constant current and power factor correction," *Electronics Letters,* vol. 50, no. 15, pp. 1086-1088, 2014.

[2] J. Park, M. Kim, S. Choi, “Zero-current switching series loaded resonant converter insensitive to resonant component tolerance for battery charger", *IET Power Electronics,* vol. 7, no. 10, pp. 2517-2524, 2014.

[3] C. S. Tang, Y. Sun, Y. G. Su, S. K. Nguang and A. P. Hu,“Determining multiple steady-state ZCS operating points of a switch-mode contactless power transfer system," *IEEE Transactions on Power Electronics,* vol. 24, no. 2, pp. 416-425, 2009.

[4] T. S. Chan and C. L. Chen, “A primary side control method for wireless energy transmission system," *IEEE Transactions on Circuits Systems I, Reg. Papers,* vol. 59, no. 8, pp. 1805-1814, 2012.

[5] T. Qian, “A converter combination scheme for efficiency improvement of PV systems," *IEEE Transactions on Circuits Systems II, Exp. Briefs, early access*, 2017, DOI:10.1109/TCSII.2017.2764027.

[6] V. Volpérian, “Approximate small-signal analysis of the series and the parallel resonant converters," *IEEE Transactions on Power Electronics,* vol. 4, no. 1, pp. 15-24, 1989.

[7] Pinheiro, H., Jain, P.K., and Joos, G., “Self-sustained oscillating resonant converters operating above the resonant frequency," *IEEE Transactions on Power Electronics,* vol. 14, no. 5, pp. 803-815, 1999.

[8] R. Bonache-Samaniego, C. Olalla and L. Martinez-Salamero, “Design of self-oscillating resonant converters based on a variable structure systems approach," *IET Power Electronics,* vol. 57, no. 1, pp. 111-119, 2015.

[9] R. Bonache-Samaniego, C. Olalla and L. Martinez-Salamero, “Dynamic Modeling and Control of Self-Oscillating Parallel Resonant Converters Based on a Variable Structure Systems Approach," *IEEE Transactions on Power Electronics,* vol. 32, no. 2, pp. 1469-1480, 2017.

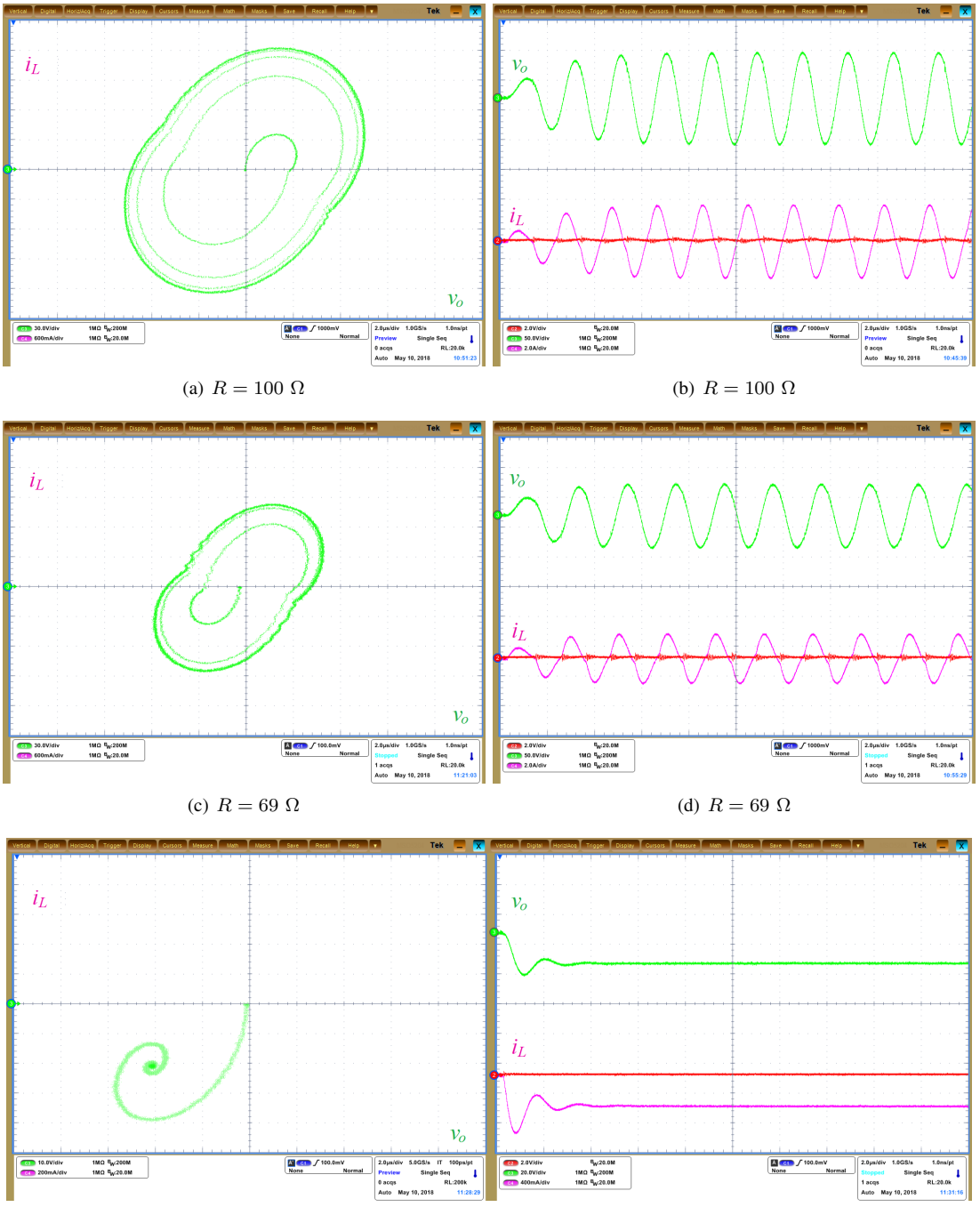

(a) $R = 100\ \Omega$ (b) $R = 100\ \Omega$

(c) $R = 69\ \Omega$ (d) $R = 69\ \Omega$

(e) $R = 54\ \Omega$ (f) $R = 54\ \Omega$

Fig. 8. Experimental state plane trajectories corresponding to Fig. 6 and their corresponding waveforms of the state variables. For the case $R = 54\ \Omega$, the system cannot reach the desired crossing limit cycle with zero initial conditions.

[10] D. Williams, C. Bingham, M. Foster, D. Stone, "Hamel locus design of self-oscillating DC-DC resonant converters," *IET Power Electronics,* vol. 3, no. 1, pp. 86-94, 2010.

[11] V. M. Hernandez, R. Silva, H. Sira-Ramirez, "On the stability of limit cycles in resonant DC-to-DC power converters," *Proc. of the 42nd IEEE Conf. on Decision and Control,* pp. 1141-1146, 2003.

[12] O. Dranga, B. Buti, and I. Nagy, "Stability analysis of a feedback-controlled resonant DC-DC converter," *IEEE Transactions on Industrial Electronics,* vol. 50, no. 1, pp. 141-152, 2003.

[13] V. I. Utkin, Variable structure systems with sliding modes, *IEEE Transactions on Automatic Control,* vol. 22, no.2, pp. 212-222, 1977.

[14] V. I. Utkin, Sliding Modes and their Application in Variable Structure Systems. Moscow, U.S.S.R.: MIR, 1978.

[15] M. di Bernardo, K. H. Johansson, and F. Vasca, "Self-oscillations and sliding in relay feedback systems: Symmetry and bifurcations," *International Journal of Bifurcation and Chaos,* vol. 11, no. 4, pp. 1121-1140, 2000.

[16] A. F Filippov, Differential Equations with discontinuous righthand sides, *Kluwer Academic Publishers,* Dortrecht, 1998.

[17] R. L. Leine and H. Nijemeijer, *Dynamics and bifurcations of non-nmooth mechanical systems,* Lecture Notes in Applied and Computational Mechanics, Vol. 18, *Springer,* 2004.

[18] L. Benadero, E. Ponce, A. El Aroudi and L. Martinez-Salamero, "Analysis of coexisting solutions and control of their bifurcations in a parallel LC resonant inverter," 2017 *IEEE International Symposium on Circuits and Systems,* (ISCAS), Baltimore, MD, pp. 1-4, 2017.

[19] E. Ponce, L. Benadero, A. El Aroudi and L. Martinez-Salamero, "Sliding bifurcations in resonant inverters," *14th International Multi-Conference on Systems, Signals & Devices,* (SSD), Marrakech, pp. 122-127, 2017.
[20] L. Benadero, E. Ponce, A. El Aroudi and F. Torres, "Limit cycle bifurcations in resonant LC power inverters under zero current switching strategy," *Nonlinear Dynamics,* vol. 91 no.2, pp. 1145-1161, 2018.
[21] R. W. Erickson and D. Maksimovic, *Fundamentals of power electronics*. Lluwer, Springuer, 2001.
[22] Ehsani, M., "Power conversion using zero current soft switching," U.S. Patent 5 287 261, 1994.
[23] M. R. Jeffrey, S.J. Hogan, "The geometry of generic sliding bifurcations," *SIAM Rev.,* vol. 53, no. 3, pp. 505-525, 2011.
[24] D. J. Pagano, E. Ponce and F. Torres, "On Double boundary equilibrium bifurcations in piecewise smooth planar systems," *Qualitative Theory of Dyn. Systems,* vol. 10, pp. 277-301, 2011.
[25] D. Giaouris, S. Banerjee, B. Zahawi, V. Pickert, "Stability analysis of the continuous-conduction-mode buck converter via Filippov's method," *IEEE Transactions on Circuits and Systems I: Regular Papers,* vol. 55, no. 4, pp. 1084-1096, 2008.

Abdelali El Aroudi (M'00, SM'13) received the graduate degree in physical science from Facultt'e des sciences, Université Abdelmalek Essaadi, Tetouan, Morocco, in 1995, and the Ph.D. degree (hons) in applied physical science from Universitat Polit'ecnica de Catalunya, Barcelona, Spain in 2000. During the period 1999-2001 he was a Visiting Professor at the Department of Electronics, Electrical Engineering and Automatic Control, Technical School of Universitat Rovira i Virgili (URV), Tarragona, Spain, where he became an associate professor in 2001 and a full-time tenure Associate Professor in 2005. His research interests are in the field of structure and control of power conditioning systems for autonomous systems, power factor correction, stability problems, nonlinear phenomena, chaotic dynamics, bifurcations and control. He served as a Guest Editor of the IEEE JOURNAL on EMERGING and SELECTED TOPICS IN CIRCUITS AND SYSTEMS Special Issue on Design of Energy-Efficient Distributed Power Generation Systems (September 2015) and a Guest Editor of the IEEE TRANSACTIONS ON CIRCUITS AND SYSTEMS Special Issue Special Issue on the 2018 IEEE International Symposium on Circuits and Systems (May 2018). He currently serves as Associate Editor in IEE IET POWER ELECTRONICS, IEE IET SYSTEMS AND DEVICES and IEE IET ELECTRONICS LETTERS.

Luis Benadero was born in Ciudad Real, Spain, in 1952. He received the Ph.D. degree from the Universitat Politécnica de Catalunya (UPC), Catalonia, Barcelona, in 1983. He is Associate Professor, at the same university, with the Applied Physics Department and formerly he was with the Department of Electronic Engineering. His research activity is related to nonlinear phenomena, currently mainly focused in nonlinear dynamics, more specifically dealing with piecewise smooth systems. Such systems have an important application in power electronics, subject in which he has published several papers in the two last decades.

Enrique Ponce was born in Seville, Spain, on July 2, 1955. He received the Ingeniero Industrial and Doctor Ingeniero Industrial degrees from the University of Seville, Seville, Spain, in 1978 and 1987, respectively. Since 1978, he has been with the Department of Applied Mathematics at the University of Seville, where he is currently a Professor. His research interests are nonlinear oscillations, bifurcations and piecewise linear systems, with emphasis on applications in nonlinear control and electronics.

Carlos Olalla (S'06, M'09) obtained the M.S. degree in electronics engineering from Universitat Rovira i Virgili, Tarragona, Spain, in 2004, and the Ph.D. degree in advanced automatic control from Universitat Politècnica de Catalunya, Barcelona, Spain, in 2009. In 2007 and 2009, he was a visiting scholar at the *Laboratoire d'Analyse et d'Architecture des Systèmes* (LAAS-CNRS), Toulouse, France, where he also held a postdoctoral position until March 2010. From 2010 to 2012 he was a visiting scholar and a research associate in the Colorado Power Electronics Center (CoPEC), University of Colorado, Boulder, USA. Since 2013, he has held several competitive postdoctoral fellowships in the Dept. of Electrical, Electronics and Automatic Control Engineering of Universitat Rovira i Virgili, where he carries out research on the modeling, optimization and robust control of power converters and renewable energy systems. last decades.

Francisco Torres was born in Puerto de Santa Maria, Spain, on September 12, 1954. He received the Licenciado en Físicas degree in 1977 and the Doctor en Ciencias Físicas degree in 1989, both from the University of Sevilla, Seville, Spain. Since 1978, he has been with the Departamento de Matemática Aplicada II at the Uniersity of Sevilla, where he is currently a Professor. His esearch interests are piecewise linear systems, bifurcation theory and dynamical systems.

Luis Martínez-Salamero received the Ingeniero de Telecomunicación degree in 1978 and the Ph.D. degree in 1984, both at the Universidad Politécnica de Cataluña, Barcelona, Spain. From 1978 to 1992, he taught circuit theory, analog electronics and power processing at the Escuela Técnica Superior de Ingenieros de Telecomunicación , Barcelona, Spain. From 1992 to 1993, he was a visiting professor at the Center for Solid State Power Conditioning and Control, Department of Electrical Engineering, Duke University, Durham, NC. From 2003 to 2004, 2010 to 2011, and March-September 2018 he was a visiting scholar at the Laboratory of Architecture and Systems Analysis (LAAS), National Agency for Scientific Research (CNRS), Toulouse, France. Since 1995 he has been a full professor with the Department of Electrical Electronic and Automatic Control Engineering , School of Electrical and Computer Engineering, Rovira i Virgili University , Tarragona, Spain, where he managed the Research Group in Automatic Control and Industrial Electronics (GAEI) in the period 1998-2018. His research interests include structure and control of power conditioning systems, namely, electrical architecture of satellites and electric vehicles, as well as nonlinear control of converters and drives, and power conditioning for renewable energy.